UDK 621.791:669.715
Original scientific article/Izvirni znanstveni članek

ISSN 1580-2949
MTAEC9, 46(3)215(2012)

FRICTION-STIR WELDING OF HIGH-STRENGTH ALUMINIUM ALLOYS AND A NUMERICAL SIMULATION OF THE PLUNGE STAGE

VRTILNO TORNO VARJENJE VISOKOTRDNIH ALUMINIJEVIH ZLITIN IN NUMERIČNA SIMULACIJA FAZE TALJENJA

Milenko Perovic[1], Darko Veljic[2], Marko Rakin[3], Nenad Radovic[3], Aleksandar Sedmak[4], Nikola Bajic[2]

[1]Chamber of Economy of Montenegro, Podgorica, Montenegro
[2]IHIS Science & Technology Park Zemun, Belgrade, Serbia
[3]Faculty of Technology and Metallurgy, University of Belgrade, Serbia
[4]Faculty of Mechanical Engineering, University of Belgrade, Serbia
mperovic@pkcg.org

Prejem rokopisa – received: 2011-09-12; sprejem za objavo – accepted for publication: 2012-01-27

This paper defines a set of welding parameters for the Friction-Stir Welding (FSW) of two forged panels of the alloy EN AW 7049A in a T652 temper and discusses the plunge stage of FSW using numerical modeling. This multi-component aluminum alloy is characterized by high strength, reduced plasticity and poor weldability. Observations of the macrostructure and microstructure clearly showed typical zones of a FSW joint and the appropriate grain sizes. The finest grains were observed within the nugget, while the coarsest grains are found to be in the HAZ. The ultimate tensile strength is 80.3 % of the parent material. A coupled thermo-mechanical model was developed to study the temperature fields and the plunge force of the alloy EN AW 7049A under different rotating speeds, (300, 400 and 500) r/min, during the FSW process of the plunge stage. A three-dimensional FE model has been developed in ABAQUS/Explicit using the arbitrary Lagrangian–Eulerian formulation, the Johnson–Cook material law and Coulomb's Law of Friction. Numerical results indicate that the maximum temperature in the FSW process can be increased with an increase in the rotational speed, which can be used to reduce the plunge force.

Keywords: friction-stir welding, welding parameters, metallography, mechanical test, numerical simulation, plunge stage, temperature, force

V članku je opisana vrsta parametrov za vrtilno torno varjenje (FSW) dveh kovanih panelov iz zlitine EN AW 7049A, popuščene po T652, in talilna faza FSW z uporabo numeričnega modeliranja. Za to večkomponentno aluminijevo zlitino so značilne visoka trdnost, majhna plastičnost in slaba varivost. Opazovanja makro- in mikrostrukture so jasno pokazala tipične cone FSW-spoja in ustrezne velikosti zrn. Raztržna trdnost je pri 80,3 % trdnosti osnovnega materiala. Povezan termomehanski model je bil razvit za raziskovanje temperaturnih polj in silo taljenja EN AW 7049A-zlitine pri različnih hitrosti vrtenja (300, 400 in 500) r/min med vrtilnim tornim varjenjem za talilno fazo FSW-procesa. Tridimenzionalni FE-model je bil razvit v ABAQUS/Explicit z uporabo arbitrarne Lagrange-Eulerjeve formulacije, Johnson-Cookovih zakonov o materialu in Coulombovega zakona o trenju. Numerični rezultati kažejo, da se lahko najvišja temperatura pri FSW-procesu poviša s povečanjem hitrosti vrtenja, ki lahko zmanjša silo potopa.

Ključne besede: vrtilno torno varjenje, varilni parametri, metalografija, mehanski preizkusi, numerična simulacija, faza taljenja, temperatura, sila

1 INTRODUCTION

Friction-Stir Welding (FSW) is a solid-state joining technique invented and patented in the late 1991 by The Welding Institute (TWI) at Cambridge, U. K.[1]

FSW is a process, in which a specially shaped cylindrical tool is rotated and plunged into the abutting edges of the parts to be welded as shown in **Figure 1**[1–3]. As the tool is moved along the joint line, the friction from the rotating tool heats the material to the extent that it plastically deforms and flows from the front of the tool to the back, where it subsequently cools and produces a weld, i.e., a weld is created by a combined action of frictional heating and mechanical deformation due to the rotating tool. The tool has a circular section except at the end where there is a threaded probe, or a more complicated flute, and the junction between the cylindrical portion and the probe is known as the shoulder. The probe penetrates the welding plate, while the shoulder rubs against the top surface. The use of FSW provides

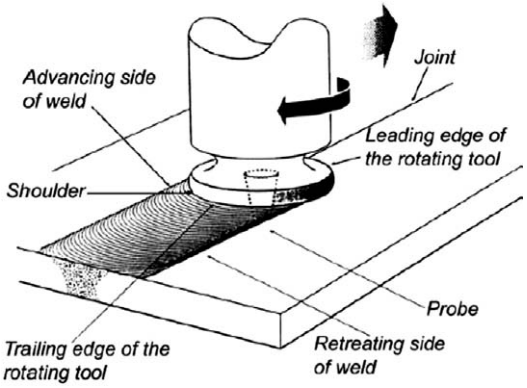

Figure 1: Schematic illustration of the FSW process[4]
Slika 1: Shematičen prikaz FSW-varjenja[4]

high-quality welds, without any void, cracking or distortion, of the materials that typically exhibit poor fusion weldability. The development of the welding technology comprises an estimation of the optimum rotation and translational speeds, with an aim to introduce the optimum heating (frictional and adiabatic). Different factors influence these parameters, like the type of the base material (a set of mechanical and physical properties), the thickness of the plates, the forging force, etc.

FSW is a very modern welding process with a great future use, primarily due to a variety of possible combinations of dissimilar materials to be welded and the possibility to be controlled efficiently. FSW can be used for joining many types of materials and material combinations: aluminum and its alloys, copper and its alloys, lead-magnesium alloys, magnesium and aluminum, zinc, titanium and its alloys, mild steel, and metal matrix composites (MMCs) based on aluminum and plastics[4].

A friction-stir weld joint in aluminum alloys consists of four major microstructural zones as shown in **Figure 2**.

The heat-affected zone (HAZ) lies close to the weld center. The material has experienced a thermal cycle, so the modifications in mechanical properties and in the microstructure are noticed. However, no plastic deformation occurs in this zone. The thermo-mechanically affected zone has been plastically deformed by the friction-stir welding tool, and the heat from the process also exerts some influence on the material. The weld nugget represents a recrystallized area in the TMAZ in aluminum alloys.

Compared with the conventional welding techniques, FSW possesses many advantages, such as the absence of melting, a low number of defects, low distortion, etc. FSW can even join thin and thick sections. The process can be applied to produce both butt and lap joints as well as T-joints. FSW is being successfully applied to the aerospace, automobile and shipbuilding industries.

The presence of defects in the form of cracks in the welded joints, caused by the melting of high-strength aluminum alloys is a very serious technological problem. It is particularly problematic in the case of the alloy series EN AW 7XXX (Al-Zn-Mg-Cu). Due to this limitation, the application of these alloys had been significantly hampered before the introduction of FSW into the mass production, at the end of the last century. The introduction of FSW has significantly improved their weldability and broadened the application of various welded components, including even some very complex elements used in the aerospace industry and in the military production. In the case of EN AW 7049A, which is a multi-component alloy of a quadruple phase composition, high strength is accomplished with the thermal precipitation based on the particles with various chemical compositions. For example, in addition to improving the hardness of the alloy, an addition of copper also results in improved plasticity, resistance to fatigue and stress corrosion[6].

The aim of this paper is to suggest the parameters for experimental welding of two forged panels made of the EN AW 7049A alloy in a T652 temper and to evaluate the plunge stage by using numerical modelling.

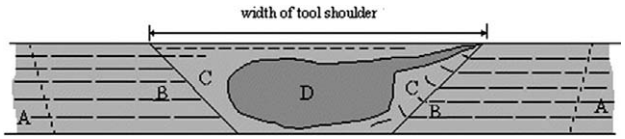

Figure 2: Microstructure of the transverse cross-section.[5] A: Base material/unaffected material, B: Heat-affected zone (HAZ), C: Thermo-mechanically affected zone (TMAZ), D: Weld nugget (Part of the thermo-mechanically affected zone)

Slika 2: Mikrostruktura na prečnem prerezu.[5] A: osnovni material, B: toplotno vplivana cona (HAZ), C: termomehansko vplivana cona (TMAZ), D: varilni koren (del termo-mehansko vplivane cone)

2 EXPERIMENT – FSW

2.1 Preparation of the welding plate

Friction-stir welding is conducted on thermally processed and machine prepared forged elements with

Figure 3: Thermally processed and machine prepared forged elements for FSW with the dimensions of 180 mm × 65 mm × 5 mm

Slika 3: Termično procesirane, obdelane pripravljene kovane plošče dimenzije 180 mm × 65 mm × 5 mm, pripravljene za FSW

Figure 4: Specimen for sample making with the dimensions of 680 mm × 580 mm × 13 mm

Slika 4: Plošča za pripravo vzorcev dimenzij 680 mm × 580 mm × 13 mm

the dimension of 180 mm × 65 mm × 5 mm (**Figure 3**), made of an alloy produced in commercial industrial conditions. A specimen for sample making was a panel with the dimensions of 680 mm × 580 mm × 13 mm (**Figure 4**), a hardness of 175 HB, and made of raw aluminium, where the alloying elements were added as clean metal alloys, or master alloys. It passed all phases of the technological procedure: thermo-mechanical processing, casting of a raw billet, two-level homogenisation, cutting and preparation for forging, free forging and forging in a tool, hardening, pressing of 1 % and 3 %, and artificial ageing.

To eliminate the potential heat influence on the initial microstructure and on the experimental results, the panels were cut with a water jet and afterwards skimmed of saw chips, and made in specified measurements with an intensive cooling of the treated surface.

2.2 Material properties

The chemical composition of EN AW 7049A-T652 aluminium, obtained by using an OE quantometer ARL with electronic samples "Pechiney", is as follows: Aluminum (Al) – Balance, Cu – 1.45, Mg – 2.15, Mn – 0.27, Fe – 0.23, Si – 0.10, Zn – 7.20, Ti – 0.015, Cr – 0.13, Zr – 0.13, V – 0.004, B – 0.003. The thermal and mechanical properties used in this model are given in **Table 1**.

Table 1: Mechanical characteristics of the parent material EN AW 7049A[7]
Tabela 1: Mehanske lastnosti osnovnega materiala EN AW 7049A[7]

Material properties	Value
Young's Modulus of Elastic (GPa)	71.7
Poisson's Ratio	0.33
0.2 % Yield Strength $R_{0.2}$/MPa	570
Tensile Strength R_m/MPa	650
Thermal Conductivity (W/(m K))	130
Coefficient of Thermal Expansion ($°C^{-1}$)	24.7×10^{-6}
Density (kg/m³)	2810
Specific Heat Capacity (J/(kg °C))	960
Temperature Melt (°C)	477
Elongantion A, %	7.5

2.3 Equipment for the procedure implementation, tools and process parameters

Experimental welding was performed with an adapted machine tool – a universal vertical milling machine, with the power of the electromotor driving the vertical milling-machine arbor being 18 kW, a gradual setting of the number of revolutions being between 80 r/min and 1450 r/min and the traverse speed ranging from 12.4 mm/min to 175 mm/min. The image of the machine is given in **Figure 5**. The backing plate with the dimensions of 300 mm × 200 mm × 25 mm (**Figure 6**), made of quenched and tempered steel 42CrMo4, thermally processed at 850 MPa and surface tempered at

Figure 5: Tool for the friction-stir welding with a backing plate on water desk
Slika 5: Orodje za vrtilno torno varjenje s podporno ploščo na vodni mizi

Figure 6: Backing plate
Slika 6: Podporna plošča

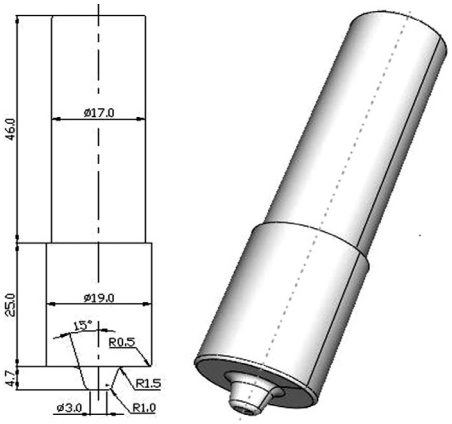

Figure 7: Welding tool used for the experiment and numerical analysis
Slika 7: Varilno orodje, uporabljeno za preizkuse in numerično analizo

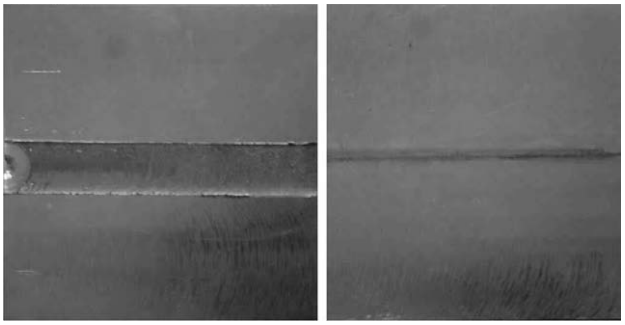

Figure 8: Photographic presentation of the face and the reverse of a welded joint
Slika 8: Posnetek prednje in hrbtne strani zvarjenega spoja

(44 ± 2) HRc, was fastened to a workbench with an improvised machine for FSW. The welding tool was inserted in the fastened head of the main milling-machine arbor and it is presented in **Figure 7**. The material of the tool is steel x155CrVMo121. The tool was thermally treated up to the surface hardness of (61 ± 1) HRc.

The pieces were fastened to the backing plate without turning down the edges and after that the vertical head of the milling machine, with the inserted tool in the tapered elastic capsule, was placed in the contact position on the central line of the joined pieces. All the process parameters were held constant during the welding. The welding parameters in the plunge phase were as follows: the plunge speed was 12 mm/min, the plunge depth of the pin was 4.9 mm, the plunge depth of the shoulder was 0.2 mm, the rotation speed was 400 r/min, the plunge time was 24.5 s. The welding parameters in the linear welding phase were as follows: the plunge depth of the shoulder was 0.2 mm, the rotation speed was 400 r/min, and the welding speed was 24 mm/min.

The welded experimental panel, whose appearance after the welding is presented in **Figure 8**, was tested on a hypersonic device with a flat probe and with the beam-transmission direction going from the bottom side towards the face of the metal weld in order to find any possible occurance of a metal discontinuity in the sample.

2.4 Mechanical testing of a welded joint of EN AW 7049A T652

The tensile test is conducted in accordance with the standard MEST EN 10002-1:2008 on the machine INSTRON 105. The test results obtained from the specimens taken normally from the welding direction are given in **Table 2**. The yield point is an apparent value measured at the elongation of 0.2 %. The tensile strength of a welded joint is about 20 % lower than that of the parent material and the apparent yield stress is almost a third bigger in the parent material than in a welded joint. The crack location of a specimen on the tension test is situated in the transition zone going from the nugget to the remaining zone of the thermomechanically affected zone.

Table 2: Mechanical characteristics of the welded joint of EN AW 7049A T652
Tabela 2: Mehanske lastnosti zvarjenega spoja EN AW 7049A T652

Trial number	Mechanical properties		
	$R_{0.2}$ /MPa	R_m/MPa	A/%
1	384	522	9.5

2.5 Microstructural evaluation

Due to the etching in the Keller's reagent, the macrostructure of the welded metal was clearly differentiated, as shown in **Figure 8**. The advancing and the retreating sides of the two regions, right and left from the centre of the welded joint, are also clearly visible. These are the

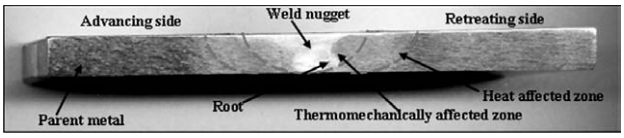

Figure 9: Macrostructure of a FSW joint
Slika 9: Makrostruktura FSW-spoja

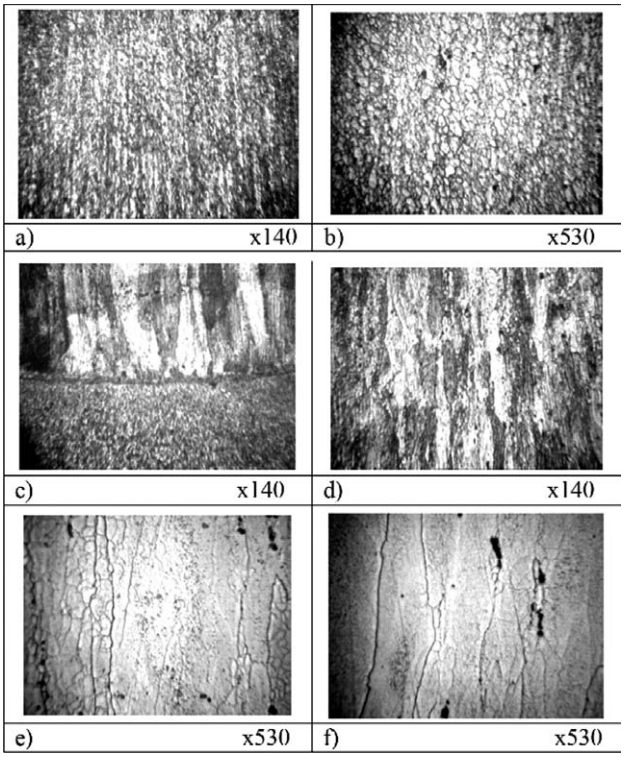

Figure 10: Microstructures obtained in a weld joint of a FS welded EN AW 7049A T652 alloy: a) weld root, b) nugget, c) transition zone between the nugget area and the thermomechanical influence, d) thermomechanicly affected zone, e) heat affected zone and f) base material zone
Slika 10: Mikrostruktura v zvarjenem FSW-spoju zlitine EN AW 7049A T652: a) koren zvara, b) jedro, c) prehod med jedrom in področjem termomehanskega vpliva, d) cona termomehanskega vpliva, e) cona toplotnega vpliva in f) osnovni material

side, where the directions of the tool-rotation vector and the welding-speed vector overlap, and the side where they have opposite directions. The macrostructure consists of the thermomechanically affected zone, the heat affected zone and the base metal zone, as shown in **Figure 9**. The thermomechanically affected zone (TMAZ) has two recognizable areas: the weld nugget and the weld root although there are authors who consider the nugget zone to be separate from the welded joint, including the root as its part.

A metallographic analysis of the sample was executed with the light microscope NEOPHOT 21 having magnifications of 100-times and 1000-times. The thermomechanically affected zone in the nugget and the root region is situated at the place of the pin-tool traverse and immediately underneath its top. This is a fine-grained recrystalized zone, slightly displaced toward the back side, as shown in **Figures 10a** and **b**. The transition region of these areas in the thermomechanically affected zone is clearly visible even with small magnifications: small equiaxed grains are in the nugget, while the larger grains are placed within the TMAZ, as shown in **Figure 10c**. The remaining part of the TMAZ zone is dominantly characterized with deformed grains and its structure consists of larger grains, shown in **Figure 10d**. The neighbouring, heat affected zone (HAZ), is characterized with the elongated grains with little recrystallized grains and with a series of intermetallic phases, shown in **Figure 10e**. Its microstructure is very simillar to the microstructure of the base material, shown in **Figure 10f**.

3 MODEL DESCRIPTION

A coupled thermo-mechanical three-dimensional FE model has been developed in ABAQUS/Explicit using the arbitrary Lagrangian–Eulerian formulation and the Johnson–Cook material law. The contact forces are modelled with Coulomb's Law of Friction, making the contact condition highly solution dependent[8–12].

3.1 Geometry, boundary conditions and the finite-element mesh

The dimension of the welding plate in the numerical model of the plunge stage is 50 mm × 50 mm × 5 mm. The three-dimensional numerical model is based on the C3D8RT element type, which is a thermo-mechanically coupled hexahedral element with 8-nodes, each having trilinear displacement and temperature degrees of freedom. This element produces a uniform strain (the first-order reduced integration) and contains hourglass control[12]. The mesh consists of 23608 nodes and 20972 elements. The tool and the backing plate are modeled as a rigid surface having no thermal degrees of freedom. The main tool geometry in the FE model is similar to the experimental tool shown in **Figure 6**. The numerical model of the welding plate, the tool and the backing plate is shown in **Figure 11**.

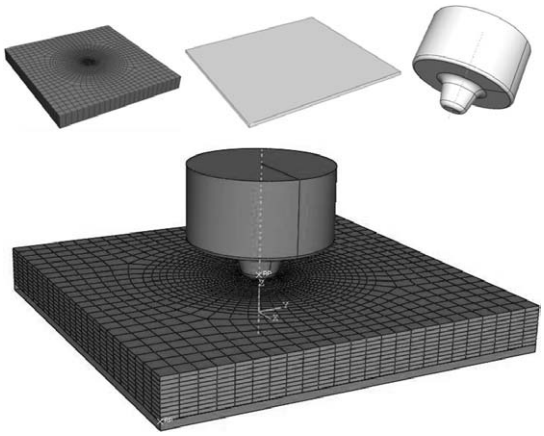

Figure 11: Numerical model of the welding plate, the tool and the backing plate

Slika 11: Numerični model varilne plošče, orodje in podporna plošča

3.2 Thermal model

In general, heat generation comes from two sources: the frictional heating at the tool welding plate interface and the plastic energy dissipation due to shear deformation in the nugget zone. The governing equation for the heat-transfer process during the plunge phase of the FSW process can be written as:

$$\rho c \frac{\partial T}{\partial t} = \frac{\partial T}{\partial x}\left[k_x \frac{\partial T}{\partial x}\right] + \frac{\partial T}{\partial y}\left[k_y \frac{\partial T}{\partial y}\right] + \frac{\partial T}{\partial z}\left[k_z \frac{\partial T}{\partial z}\right] + \dot{q}_p \quad (1)$$

where ρ is the density, c is the specific heat, k is the heat conductivity, T is the temperature, t is the time, $\dot{q}_p$ is the heat generation coming from the plastic energy dissipation due to shear deformation, and x, y, and z are spatial coordinates[12–17]. The rate of the heat generation due to the plastic energy dissipation, $\dot{q}_p$, is computed from:

$$\dot{q}_p = \eta \sigma \dot{\varepsilon}^{pl} \quad (2)$$

where η is the factor of converting mechanical to thermal energy (0.9)[12], σ is the shear stress, and $\dot{\varepsilon}^{pl}$ is the rate of the plastic strain. The heat generation caused by the frictional heating between the tool and the work pieces can be written as:

$$\dot{q}_f = \frac{4}{3}\pi^2 mPNR^3 \quad (3)$$

where $\dot{q}_f$ is the frictional heat generation, μ is the coefficient of friction, P is the traction, N is the rotational speed and R is the surface radius.

3.3 Johnson-Cook elastic–plastic model

In the thermo-mechanically affected zone (TMAZ) a very large deformation takes place during the process. The interaction of the flow stress with the temperature, the plastic strain and the strain rate is essential for

modeling the FSW process. For this reason the Johnson-Cook elastic–plastic model is selected. The formulation for this model is empirically based. The elastic–plastic Johnson–Cook material law is given by[9]:

$$\sigma_y = \left[A + B(\varepsilon_p)^n\right] \cdot \left[1 + C\left(\frac{\dot{\varepsilon}_p}{\dot{\varepsilon}_0}\right)\right] \cdot \left[1 - \left(\frac{T - T_{\text{room}}}{T_{\text{melt}} - T_{\text{room}}}\right)^m\right] \quad (4)$$

where T_{melt} = 477 °C is the melting point or the solidus temperature, T_{room} = 20 °C is the ambient temperature, T/°C is the effective temperature, A = 570 MPa is the yield stress, B = 350 MPa is the strain factor, n = 0.4 is the strain exponent, m = 1.5 is the temperature exponent, C = 0.12 the strain rate factor. A, B, C, n, T_{melt}, T_{room} and m are the material/test constants for the Johnson–Cook strain-rate dependent yield stress for 7049A T652[12].

4 RESULTS AND DISCUSSION

The analysis of the experimental welding of the forged panels of alloy EN AW 7049A in the state of the maximum-hardness values (T652) showed that the elongation of the welded joint is bigger than that of the parent material, which can be explained with the formation of a structure with small grains in the mixed zone.

A coupled thermo-mechanical model was developed to study the temperature fields and the plunge force of alloy EN AW 7049A under different rotating speeds: (300, 400 and 500) r/min during the FSW process of the plunge stage. **Figure 11** shows the coordinates of point T(9.5, 0, 0) used for measuring the temperature dependence of the time.

The heat transfer through the bottom surface of the welding plate is controlled with the heat transfer coefficient of 1000 W/(m^2 K). A constant friction coefficient of 0.3 is assumed between the tool and the welding plate and the penalty contact method is used to model the contact interaction between the two surfaces. The heat convection coefficients on the surface of the welding plate are h = 10 W/(m^2 K) with the ambient temperature of 200 °C [9]. **Figure 12** shows the temperature fields in the transverse cross-section near the tool/matrix interface after 22.8 s, when the plunge speed is 12 mm/min and the rotation speed is 400 r/min. The temperature field is symmetric.

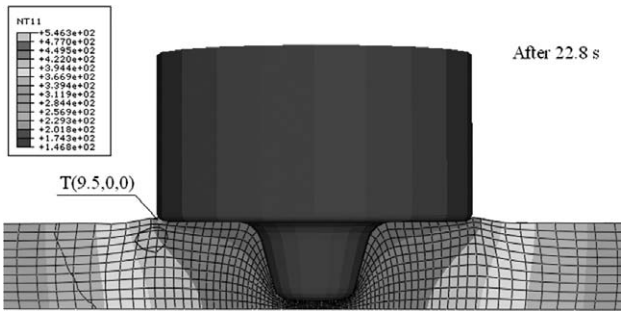

Figure 12: Temperature fields in the transverse cross-section near the tool/matrix interface after 22.8 s, when the rotation speed is 400 r/min and the plunge speed is 12 mm/min

Slika 12: Temperaturna polja na prečnem prerezu blizu mejne površine orodje – matica po 22,8 s, ko je bila hitrost vrtenja 400 r/min in hitrost trna 12 mm/min

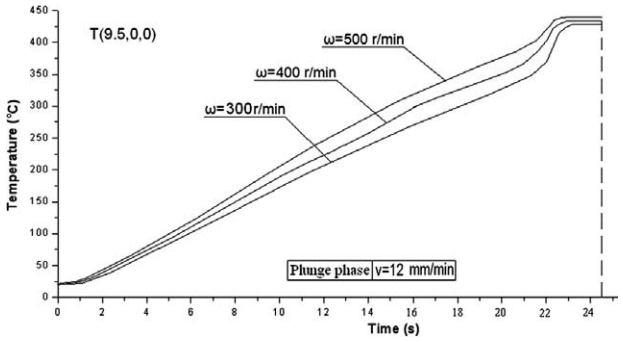

Figure 13: Temperature dependence of the time (point T) during the plunge stage

Slika 13: Razmerje med časom in temperaturo (točka T) v območju trna

Figure 13 shows the temperature dependence of the time for the plunge stage, when the rotation speeds are (300, 400 and 500) r/min in point T(9.5,0, 0).

Numerical results indicate that the temperature in the FSW process can be increased with an increase in the rotational speed and that the maximum temperature is lower than the melting point of the welding material (T_{melt} = 477 °C – **Figure 12**). The maximum temperature created by the FSW ranges from 80 % to 90 % of the melting temperature of the welding material.

Figure 14 shows the plunge-force dependence of the time during the plunge stage of the FSW process. At the start of the FSW, during the initial plunging, due to a lack of generated heat, deformation strengthening occurs, leading to an increase of force, Pos1. After establishing the contact between the rotating pin and the welding plate, the generated heat leads to an increase in the temperature. This temperature increase decreases the

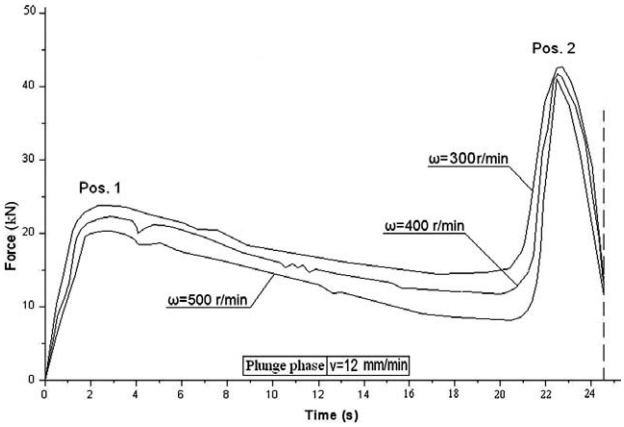

Figure 14: Force dependence of the time during the plunge stage

Slika 14: Odvisnost med silo in časom v območju trna

resistance to deformation, both though easier cross-slip and possible recovery and/or recrystallization. The resulting behavior is a decrease in force with a prolongation of time. This trend continues until the moment of contact between the tool shoulder and the welding plate when the force experiences a sharp increase, followed by an equally sharp decrease. The increase is related to the friction between the cold tool shoulder and the welding plate. Again cold deformation and work hardening occur prior to the heating introduced by the friction. The intense heat generation leads to a deformation under high temperatures, resulting in a decrease of the resistance to deformation, i.e. to a sharp fall of force.

5 CONCLUSIONS

The observations of the macrostructure and the microstructure clearly showed typical zones of a FSW joint made of the EN AW 7049A – T652 alloy. The finest grains were observed within the nugget, while the coarsest grains were found to be in the HAZ. The ultimate tensile strength was at 80.3 % of the parent material. This behaviour is related to an intense plastic-deformation influence of the heat generated due to the surface-friction plastic deformation.

The temperature in the matrix under the tool must be lower than the melting temperature. The maximum temperature created by FSW ranges from 80 % to 90 % of the melting temperature of the welding material. When the rotational speed is increased, the region of high temperature can be increased. The temperature field is symmetric. After establishing the contact between the rotating pin and the welding plate, as well as the tool shoulder and the welding plate, the force starts to increase and reaches a peak value indicated by Pos 1 and Pos 2. The force drops from Pos 1 to Pos 2 because of the material plasticity and softens due to high stress and temperature increase. When the rotational speed is increased, the plunge force can be reduced.

6 REFERENCES

[1] H. Aydin, A. Bayram, U. Esme, Y. Kazancoglu, O. Guven, Application of grez relation analysis (GRA) and taguchi method for the parametic optimization of friction stir welding (FSW) process, Mater. Tehnol., 44 (**2010**) 4, 205–211

[2] D. Veljic, Technology of Friction Stir Welding of Aluminium Alloys, M.Sc. Thesis, Faculty of Mechanical Engineering, University of Belgrade

[3] Z. W. Chen, S. Cui, Tool-workpiece interaction and shear layer flow during friction stir welding of aluminium alloys, Transaction of Nonferrous Metal Society of China, 17 (**2007**), 258–261

[4] http://www.twi.co.uk

[5] http://www.twi.co.uk/ Microstructure Classification of Friction Stir Welds

[6] M. Vratnica, Microstructural properties and mechanical properties of highly hard aluminium alloys of different grade of purity, doctoral thesis, Faculty of Technology – Metallurgy, Belgrade, Serbia, 2000

[7] The Project of production planning for the alloy PD33 – internal report – SOUR Aluminium Plant Titograd, Titograd, SFRY, 1983

[8] Z. Zhang, J. Bie, H. Zhang, Effect of Traverse/Rotational Speed on Material Deformations and Temperature Distributions in Friction Stir Welding, J. Mater. Sci. Technol., 24 (**2008**), 907–913

[9] H. Schmidt, J. Hattel, A local model for the thermo-mechanical conditions in friction stir welding, Modelling Simul. Mater. Sci. Eng., 13 (**2005**), 77–93

[10] Abaqus Inc., Analysis – User's Manual v.6.7, 2007

[11] D. Veljic, M. Perovic, B. Medjo, M. Rakin, A. Sedmak, H. Dascau, Thermo-mechanical modeling of Friction Stir Welding, The 4th International Conference, Innovative technologies for joining advanced materials, Timisoara, 2010, 171–176

[12] H. Dascau, A. Sedmak, M. Rakin, D. Veljic, M. Perovic, B. Medjo, N. Bajic, Numerical simulation of the plunge stage in friction stir welding – different tools, The 5th International Conference, Innovative technologies for joining advanced materials, Timisoara, 15, 2011, 1–4

[13] K. Park, Development and analisys of ultrasonic assisted friction stir welding process, Doctor of Philosophy (Mechanical Engineering) in The University of Michigan, 2009

[14] S. Vijay, Thermo-mechanical and Microstructural Issues in Joining Similar and Dissimilar Metals by Friction Stir Welding, A Dissertation Presented to the Graduate Faculty of Mechanical Engineering Southern Methodist University, 2006

[15] H. Zhang, Z. Zhang, J. Chen, 3D modeling of material flow in friction stir welding under different process parameters, Journal of Materials Processing Technology, 183 (**2007**), 62–70

[16] S. Guerdoux, L. Fourment, 3D numerical simulation of different phases of friction stir welding, Modelling Simul. Mater. Sci. Eng., 17 (**2009**)

[17] M. Grujicic, T. He, G. Arakere, H. V. Yalavarthy, C. F. Yen, B. A. Cheeseman, Fully coupled thermomechanical finite element analysis of material evolution during friction-stir welding of AA5083, Proceedings of the Institution of Mechanical Engineers, Part B: Journal of Engineering Manufacture, 224 (**2010**) 4, 609–625